LIMNOLOGY and OCEANOGRAPHY: METHODS

ASLO

Limnol. Oceanogr.: Methods 20, 2022, 768–780

doi: 10.1002/lom3.10521

The use of an automated organism tracking microscope in mesocosm experiments

Nicholas Blackburn,[1] Pia Haecky ,[1]* Iveta Jurgensone ,[2] Evelina Griniene,[3] Sonia Brugel,[4,5] Agneta Andersson ,[4,5] Jacob Carstensen [6]

[1]MicroWISE, Ebeltoft, Denmark
[2]Latvian Institute of Aquatic Ecology, Riga, Latvia
[3]Marine Research Institute, Klaipėda University, Klaipėda, Lithuania
[4]Department of Ecology and Environmental Science, Umeå University, Umeå, Sweden
[5]Umeå Marine Sciences Centre, Umeå University, Hörnefors, Sweden
[6]Department of Ecoscience, Aarhus University, Roskilde, Denmark

Abstract

A method for automatically counting and measuring sizes and motility behavior of zooplankton and phytoplankton in water samples is presented. Two video cameras are focused on separate optical chambers of different sizes. The chambers are filled and emptied repeatedly by synchronized pumps. Real-time motion analysis is performed by computer on the respective video feeds. Fluorescence from chlorophyll *a* (Chl *a*) is imaged at single pixel resolution. Measured parameters for individual organisms include size, swimming velocity, motility patterns, and chlorophyll fluorescence density. The system was tested during a mesocosm experiment where it was mounted on one of several mesocosm columns. The results were validated against Chl *a* measurements and microscopy counts. A sampling interval of 1 per day revealed detailed dynamics of chlorophyll activity as well as shifts in both the phytoplankton and zooplankton community structure over the course of a month. A helix coefficient, a metric related to organism motility behavior, showed substantial variation over time, consistent with changing plankton communities. Sampling rates as frequent as 1 per hour enables detailed analysis of diurnal vertical migration and similar phenomena at fixed sampling points.

Quantifying the plankton community structure and dynamics in aquatic ecosystems is desirable but not easy. Plankton recorders have been deployed in the field since 1930 and have contributed much to our understanding of the microbial food web (Table 1), but it is still a demanding task to acquire plankton community data in the field and in conjunction with experiments. It would be valuable to acquire community data on an hourly basis, but in practice, it can often only be done on a daily or even weekly basis due to the effort involved. A parameter such as chlorophyll is relatively easily measured using fluorometers and the data generally correlate well to the biomass of the phytoplankton community (Brewin et al. 2019), but without size fractionation it does not give information on community structure. The heterotrophic community is even more difficult to quantify. The most common method is to count and classify those organisms manually under the microscope. However, there are imaging sensors available for recording the plankton community (Benfield et al. 2007). Some use underwater cameras to capture images of a volume of water, while others use flow-through cuvettes to capture images of plankton as they are carried past a camera in the flow. Recent technology in holographic flow cytometry also promises light weight and low cost. *See* Table 1 for a chronological overview of methods and devices. All these methods are based on acquiring static images of plankton and then subsequently measuring and classifying them either manually or automatically by machine recognition. This final step, in particular, still represents a significant challenge and potentially high workload.

A well-known characteristic of heterotrophic organisms in nearly all size classes is their ability to swim. Manual counters often use this characteristic to determine if an organism is alive or not, but automated flow-based systems and in situ imaging sensors do not. In this study, we automatically acquire data on swimming organisms in the size range of 4–

*Correspondence: ph@microwise.eu

Additional Supporting Information may be found in the online version of this article.

Table 1. Comparison of some devices and methods for plankton enumeration and classification.

	Sample analysis			Analysis methods						
Name	Size range (μm)	Resolution (μm)	Sample rate	Static images	Motion analysis	Fluorometry	Cuvette or in situ	Weight (kg)	Year	Comments
Continuous plankton recorder (CPR)*	> 270		3000 L h^{-1}				IS		1948	Sampling onto a moving filter
Video plankton recorder (VPR)†	> 50	10–300	200–200,000 L h^{-1}	X			IS		1992	Strobe illumination, four cameras
Underwater vision profiler (UVP)‡	> 400	200	20,000 L h^{-1}	X			IS	30	2000	Semi-open glass port
Imaging flow CytoBot§	10–100	0.3	15 mL h^{-1}	X		X	C	32	2007	
Lightframe on-sight key species investigation (LOKI)‖	> 50	13	54 L h^{-1}	X			IS		2009	Semi-open glass port, optional concentrating net
Plankton imaging apparatus (PIA)¶	> 200	24	2400 L h^{-1}	X			C		2015	
Automatic litter and plankton sampler (CALPS)#	> 200		2400 L h^{-1}				IS		2016	Sampling and size fractionation by filtration
FlowCAM**	2–1000	0.025–0.5	3–300 mL h^{-1}	X		X	C	28	2016	Different optics and flow cells
FlowCAM Macro††	300–5000	1–2.5	6–54 L h^{-1}	X			C	28	2016	Different optics and flow cells
Holographic flow cytometry‡‡	25–1000	2	100 mL h^{-1}	X			C	1	2018	Holographic microscopy
BallastWISE§§	5–1000	2–20	2–1000 mL h^{-1}		X	X	C	4	2018	Two camera system

*Reid et al. (2003).
†Davis et al. (1992).
‡Picheral et al. (2010).
§Olson and Sosik (2007).
‖Schulz et al. (2009).
¶Culverhouse et al. (2015).
#Pitois et al. (2016).
**Dashkova et al. (2017).
††https://www.fluidimaging.com/products/flowcam-macro, accessed 27 June 2022.
‡‡Görögcs et al. (2018).
§§Holmstrup et al. (2020).

1000 μm (or above) using an imaging- and real-time analysis technology which is simple to use in practice and is thus low cost. The technology allows organisms to be both counted individually and categorized by their individual size and swimming speed. The same imaging system is also used to quantify chlorophyll within individual organisms using standard fluorescence techniques but at single pixel resolution, and thus allows counting and measuring both nonmotile and motile organisms containing chlorophyll. Preliminary results in the laboratory show promising correlations between the technology and proven manual microscopy methods (Holmstrup et al. 2020) and here we present how the technology performs over the course of a month in a mesocosm experiment where manual counts of the plankton community were conducted as well as measurements of chlorophyll concentrations. The aim was to test if the system could run fully automatically over the given time period, to compare it with other proven metrics in a representative environmental monitoring scenario, and to explore the advantages of high sampling rates and aspects relating swimming behavior with plankton community dynamics.

Materials and procedures

Mesocosm experiment

The experiment was carried out from 9 September to 12 October 2019, using double-mantled high-density polyethylene indoor mesocosm tanks (5 m high, 0.74 m in diameter) located at the Umeå Marine Sciences Center, Sweden (Båmstedt and Larsson 2018). On 9 September, the mesocosms were filled with 300-μm filtered brackish water pumped from two inlets located 800 m from land at water depths of 2 and 8 m. A fast convective mixing was achieved by forcing a temperature of 18°C to the top, middle and bottom sections of the mesocosm walls, resulting in a complete mixing of the mesocosm in 6 h. The overall temperature throughout the water column was subsequently maintained at 18°C. The Valoya R-258 (Light DNA) light source was set to 12 : 12 light: dark cycle from 08:00 h to 20:00 h. The photosynthetically active radiation level of the lamp was adjusted to be 330 μmol photons s^{-1} m^{-2} at 1 cm below the water surface. Air was gently bubbled just below the water surface to avoid biofilm formation and to mimic a natural wavy movement at the surface.

After 2 d of acclimation, nutrients were added in order to stimulate phytoplankton growth. The addition was performed by deploying a tube from the bottom to the top of the mesocosm to allow an even distribution of the addition. The mesocosm received nitrate ($NaNO_3$ solution) to reach a concentration of 10 μmol L^{-1} in the mesocosm and phosphate (NaH_2PO_4 solution) to reach 1 μmol L^{-1}. The nutrient concentrations were measured twice a week, and nutrients were added accordingly to maintain the nutrient target concentrations in the mesocosms.

Water samples were taken from the mesocosms two times a week for measuring nutrients and chlorophyll, and once a week for phytoplankton and zooplankton counting (Days 1, 8, 15, 22, and 29). Equal volumes were taken from the mesocosm outlets at 0.5, 1.5, and 2.3 m depth, and pooled together to represent an integrated sample of the photic zone. After each water sampling, the mesocosm tank was refilled with 0.2-μm filtered seawater to compensate for the volume lost during the sampling procedures (~ 50 and ~ 10 L for sampling including and not including plankton taxonomic determination, respectively).

Chlorophyll *a* (Chl *a*) was analyzed by spectrofluorimetry. Mesocosm water (200 mL) was filtered on 25 mm GF/F filters. The filters were frozen at −80°C and later extracted in 10 mL of 95% ethanol overnight in the dark at 4°C. The extract was analyzed on a PerkinElmer (LS 30) spectrofluorometer (at 433 nm excitation and 673 nm emission wavelengths).

Automatic counting

The measuring technology consists of two parallel optical systems, each one for measuring its respective size range. Each optical system consists of a video camera, lens, light emitting diode (LED) lights, and optical chamber (Fig. 1). The lights shine perpendicular to the optical axis to give a dark-field effect. Physical parameters are shown in Table 2. The chambers are filled and emptied by pumps. The synchronization of pumping and switching on and off the lights is facilitated by microcontroller, which opens and closes solid state relays, and which communicates with the main software program.

An analysis is performed by filling a chamber, waiting for the sample to settle within the chamber, switching on the light and starting the online video analysis. The program registers all movement by way of a background subtraction algorithm and subsequently tracks actively swimming organisms. The result is a stream of vectorized tracks, including the physical width and area of each organism at each point in time and

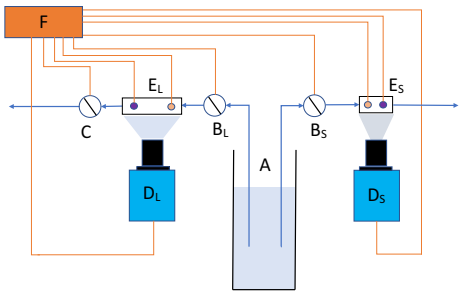

Fig. 1. Schematic of the method. A: Sample source (mesocosm column), B_L: Self-priming filling pump for large optical chamber, B_S: Self-priming filling pump for small optical chamber, C: Emptying pump, D_L: Camera for large optical chamber, D_S: Camera for small optical chamber E_L: Large optical chamber with LED lights (individually controlled), E_S: Small optical chamber with LED lights (individually controlled), F: Control unit connected to a host computer, blue lines: Water flow, Orange lines: Connecting wires.

Table 2. Physical parameters of camera and optical chambers.

	Resolution (pixels)	Pixel size (μm)	Chamber depth (mm)	Chamber volume (mL)	Organism size range (width in μm)	Video frame rate (s^{-1})
Small chamber	3000 × 2000	2.4	0.7	0.024	5–50	10
Large chamber	3000 × 2000	22	7	20	45–1000	20

space. The duration of each stream is typically 10 s. The results from 20 subsequent chamber analyses are combined to give a single analysis, representing a measured volume of 0.48 and 400 mL for the two size fractions, respectively. The data are imported into a local database for subsequent analysis. Chlorophyll within individual cells is registered in a separate pass, where the light is switched to a 420 nm purple wavelength to stimulate Chl *a* fluorescence. A 590 nm high-pass filter is placed in front of the cameras so that only fluorescence light is seen by the cameras. In this way, fluorescence density at pixel scale is imaged by the camera sensors. A different detection algorithm can be used for chlorophyll detection due to the high level of contrast, where nonmotile organisms are also detected. The wavelength of light for the first pass for pure motion detection is around 600 nm (amber), which is not blocked by the high-pass filter. The luminous power for the amber/red LEDs is approximately 80 and 30 lm for the purple LEDs, respectively, for both chamber sizes.

The physical implementation of the technology is commercially available as a measurement apparatus for quality control of ballast water for the shipping industry, BallastWISE (www.microwise.eu; Fig. 2), which consists of a box frame onto which cameras, lamps, pumps, and fixtures for optical chambers are mounted, and which are controlled by its software application.

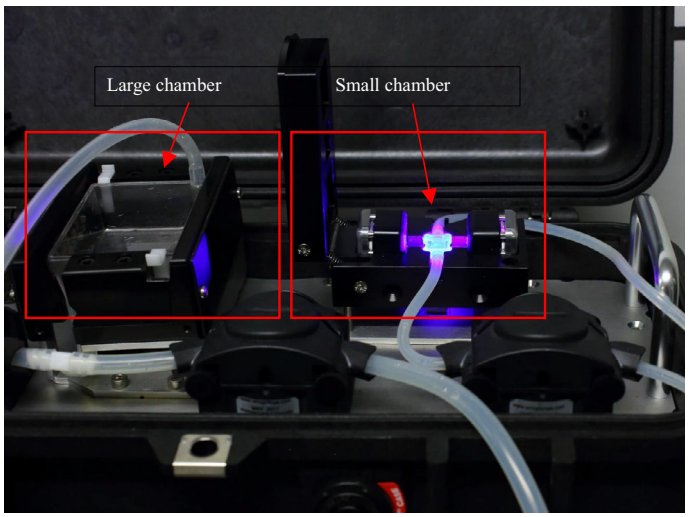

Fig. 2. Photograph of BallastWISE measuring unit. On the right side is the small chamber with attached tubes, its fixture in the open position, and with the lighting on. On the left side is the large chamber in its fixture with tubes running through the filling and emptying pumps, and the pressure-equalizing/overflow tube is seen at the top of the chamber.

In this experiment, BallastWISE was mounted on top of one of the mesocosm columns. Silicone tubes on the inlet side were led over the top edge down to a depth of approximately 80 cm below the surface. Discharge water was returned to the column. A schedule was set to perform a measurement automatically once a day and once an hour on the last day. BallastWISE has certain built-in lower size thresholds related to ballast water regulations and these were overruled for this experiment in order to include smaller organisms. Counts and swimming speeds in various size classes were extracted from the vectorized data. A database contains a record for each individual organism and for each video frame. Each record consists of a set (width, area, x, y, t), where width and area are measurements of the organism at time t; x, y are spatial coordinates at time t, and t is a timestamp for the video frame.

Manual microscopic analysis of phytoplankton

Phytoplankton samples (50 mL) were fixed with acid Lugol's solution (Willén 1962). Subsamples of 10 and 25 mL of fixed samples were settled in a sedimentation chamber for 12 h and counted according to the Utermöhl method (Utermöhl 1958) with an inverted microscope (Nikon ECLIPSE TE300) at ×200 and ×400 magnification. The number of counted cells in all subsamples exceeded 500. Phytoplankton were identified to genus or species level. Organisms were counted as cells or counting units in lengths of 100 μm for filamentous cyanobacteria. To calculate each taxon cell body volume, the best fitting geometric shape and matching equation and for biomass estimations, biovolumes, and fixed size-classes recommended in routine monitoring of the Baltic Sea phytoplankton were used (Olenina et al. 2006; HELCOM 2021*a*). The autotrophic ciliate *Mesodinium rubrum* was counted together with phytoplankton following HELCOM recommendations. Filamentous cyanobacteria were counted in lengths of 100 μm with microscopy (HELCOM 2021*a*), however to be able to compare cell abundances with the automatic counts, the 100 μm filaments were converted into cell numbers according to the taxa (HELCOM PEG biovolume file at https://helcom.fi/helcom-at-work/projects/peg/, accessed 27 June 2022). For comparison with BallastWISE data, phytoplankton organisms were grouped in four size maximum dimension fractions: < 10; 10–20; 20–50, and > 50 μm based on cell size.

Manual microscopic analysis of zooplankton

For zooplankton analysis, in total 24 L of water was filtered through a 25-μm pore size mesh plankton net and preserved in 1% Lugol's solution. Zooplankton were identified to genus or species level and counted by the Utermöhl (1958) method using an inverted microscope (Leica DM IL LED Fluo), the processed number of organisms was on average was 1000 ind./sample, ranging from 200 to 2000 ind./sample. The calanoid copepods were divided into their different developmental stages as recommended by HELCOM (2021*b*), that is, nauplii, copepodites I–III, copepodites IV–V, adult females (F) and adult males (M). Body length of cladoceran (*Bosmina coregoni*) without shell spine and total (prosome plus urosome) length of each copepod species (adult and copepodite stages) was measured at ×100 magnification, naupliar stage individuals were measured at ×200 magnification using ocular scale. Rotifer body size measurements were taken from a previous mesocosm

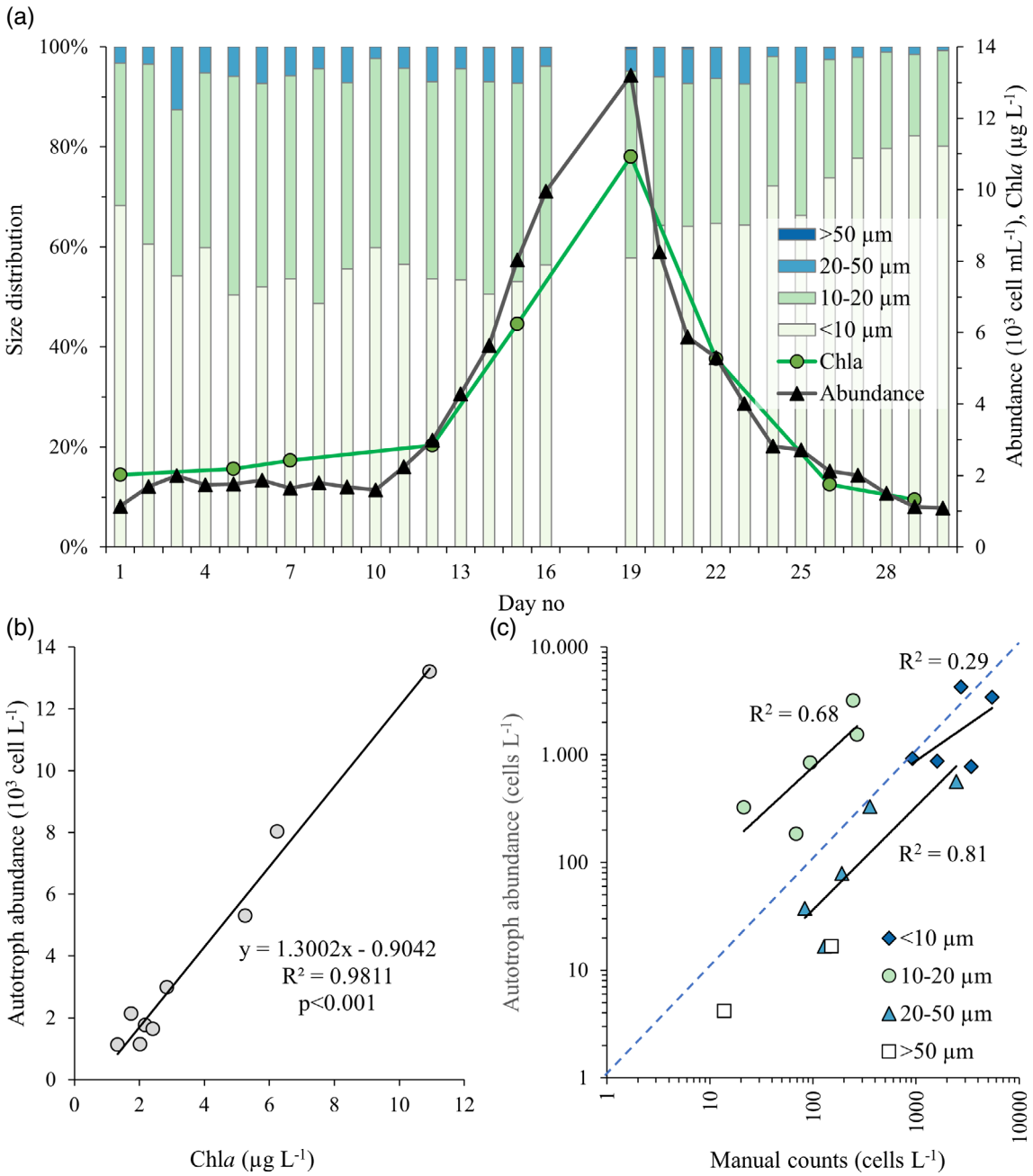

Fig. 3. (**a**) Automatic phytoplankton counts grouped into size classes together with Chl *a*; (**b**) Chl *a* correlation with automatic phytoplankton counts. (**c**) Automatic phytoplankton counts vs. manual counts grouped into size classes.

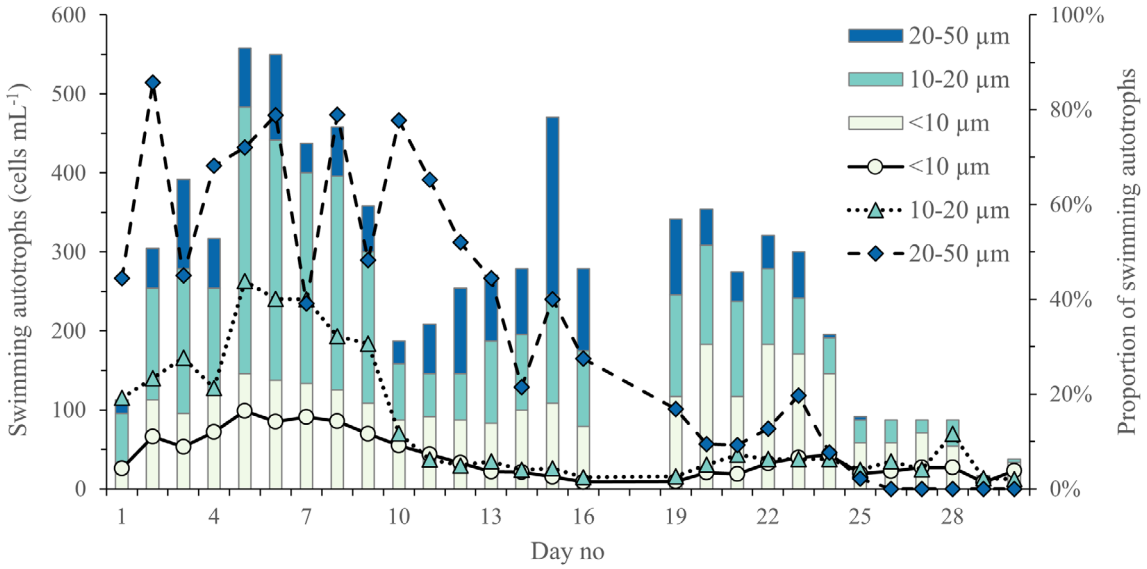

Fig. 4. The number of swimming organisms containing chlorophyll in different size classes (bar graph) and their percentage of the total population (line graphs).

study performed at Umeå Marine Sciences Center. For each species/copepod stage, 10 individuals were measured per sample. Zooplankton were grouped in three size fractions: 50–200, 200–500, and 500–800 μm based on zooplankton grouping of automatic counts. Heterotrophic ciliates were not included in the analysis.

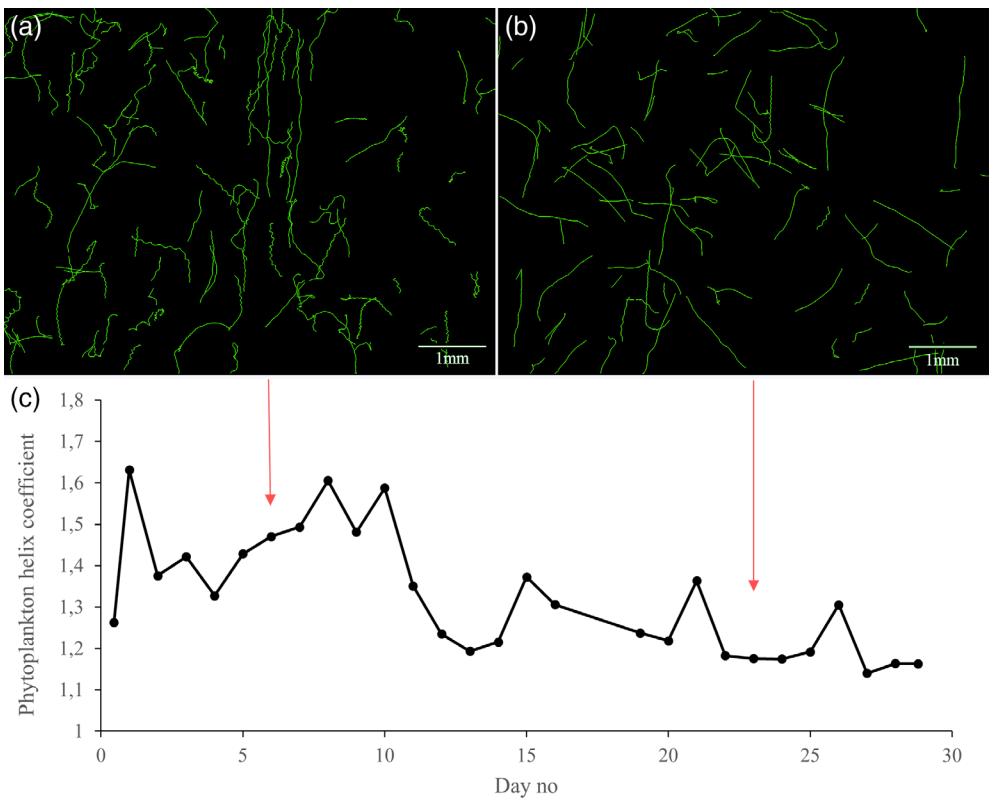

Fig. 5. Accumulated swimming tracks of phytoplankton on particular days. (a) Day 6, predominantly the chlorophyte *Pyramimonas* spp. and flagellates. (**b**) Day 23, predominantly *Chrysochromulina* spp. (**c**) Daily community averaged helix coefficient for all phytoplankton with arrows linking the swimming tracks (**a**) and (**b**) with the helix coefficient time series.

Assessment

The automatic counter ran without interference for the entire duration of the experiment (1 month), except for a power cut over the weekend around Day 17. There was no significant fouling of the optical chambers.

Phytoplankton

The number of autotrophs peaked around Day 20 in the experiment and correlated well with the chlorophyll signal ($r = 0.99$; $p < 0.001$) measured by the fluorometer (Fig. 3a,b). The manual counts missed the peak dynamics between Days 15 and 22, when there was no sampling for microscopy analysis. The phytoplankton community in the manual counts in Days 1 and 8 were dominated by small flagellates < 10 μm, while in day 15 the larger size > 20 μm diatoms, such as *Cylindrotheca closterium*, became more abundant (Supplementary Table S2). Smaller cells took over again towards the end of the experiment from Day 22 (Table S2). This trend is seen more clearly in the automatically

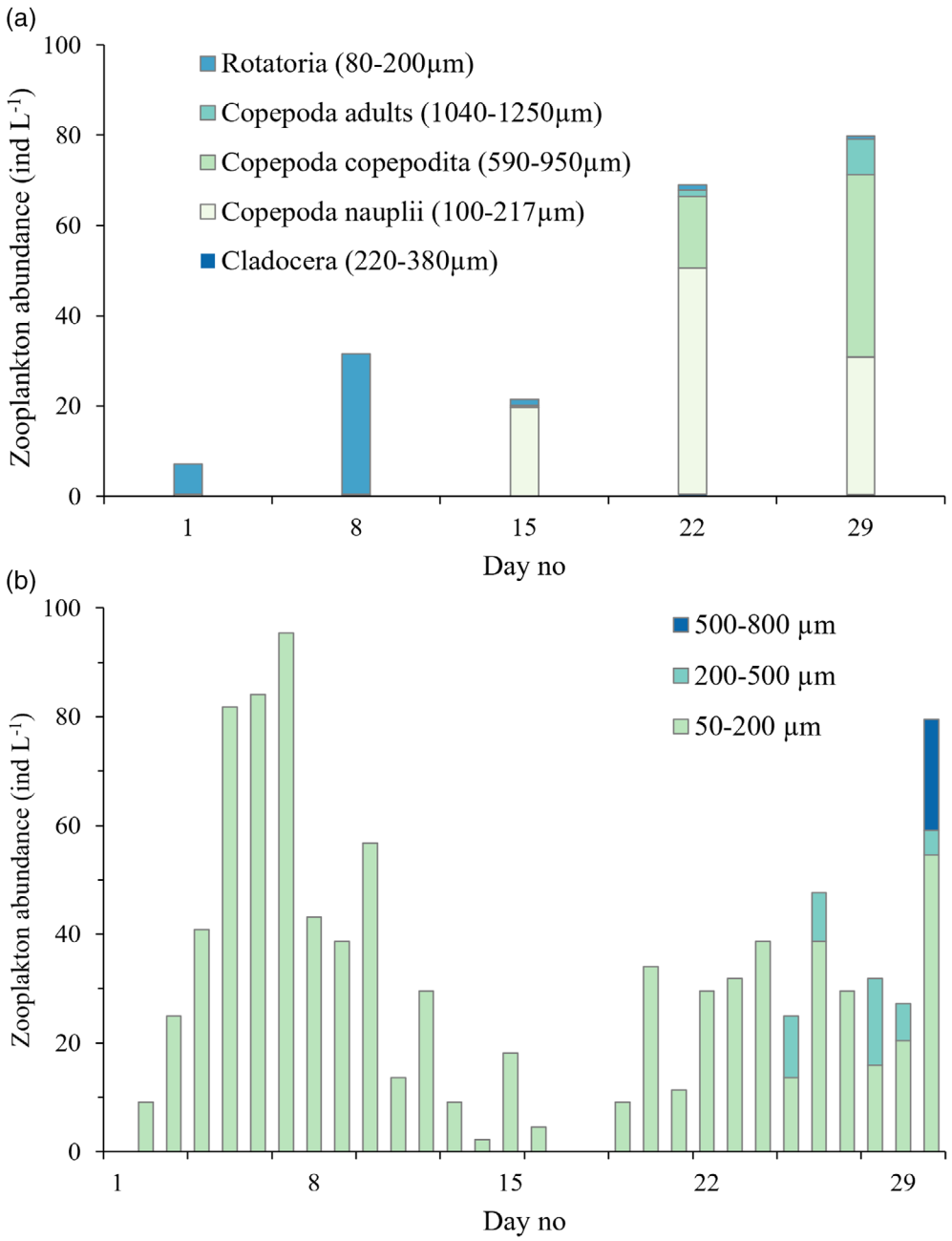

Fig. 6. Zooplankton succession over the course of the experiment assessed by manual counts divided into five taxonomical groups (**a**) and automatic counts divided into size (length) classes (**b**).

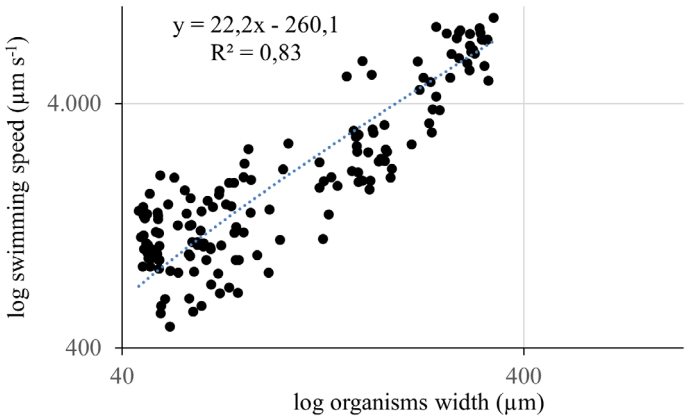

Fig. 7. Zooplankton swimming speed vs. organism size (length). Note the use of log-scales on both axes, although the regression was estimated on untransformed data.

determined size dynamics because of the higher frequency (Fig. 3a). The correlation between manual counts and automatic counts was generally good (slope = 0.87, $R^2 = 0.87$) but when divided into size classes, there was a certain amount of "spillage" between adjacent fractions (Fig. 3c) due to (1) the automatic counter only seeing chlorophyll in purely autotrophic cells, the extent of which can be smaller than the cell itself, (2) cells in colonies may be concatenated into one larger entity, and (3) larger cells with distributed chloroplasts can be split into smaller sized entities.

The shift in community structure towards diatom dominance in the middle of the experiment can also be seen in the declining proportion of motile cells from Day 10 (Fig. 4).

After Day 19, a new community structure was established with less motile organisms in all size classes (Fig. 4), and a motile community dominated by the haptophyte *Chrysochromulina* spp. (Supplementary Table S2). Swimming tracks during the first and last part of the experiment (Days 1–10 and Days 19–30, respectively) exhibited significant differences. The predominantly spiral shaped patterns on Day 6 (Fig. 5a) were replaced by more straight swimming patterns on Day 23 (Fig. 5b). This can be quantified by calculating a "helix coefficient," defined at the integrated distance swum divided by the distance moved from the start location to the end location (Fig. 5c). A high helix coefficient value corresponds to a more convoluted swimming track or tight spiral and a low value corresponds to a straighter swimming track. A phototactic response is also visible in the swimming tracks as the light source is from the top and many tracks are vertically oriented.

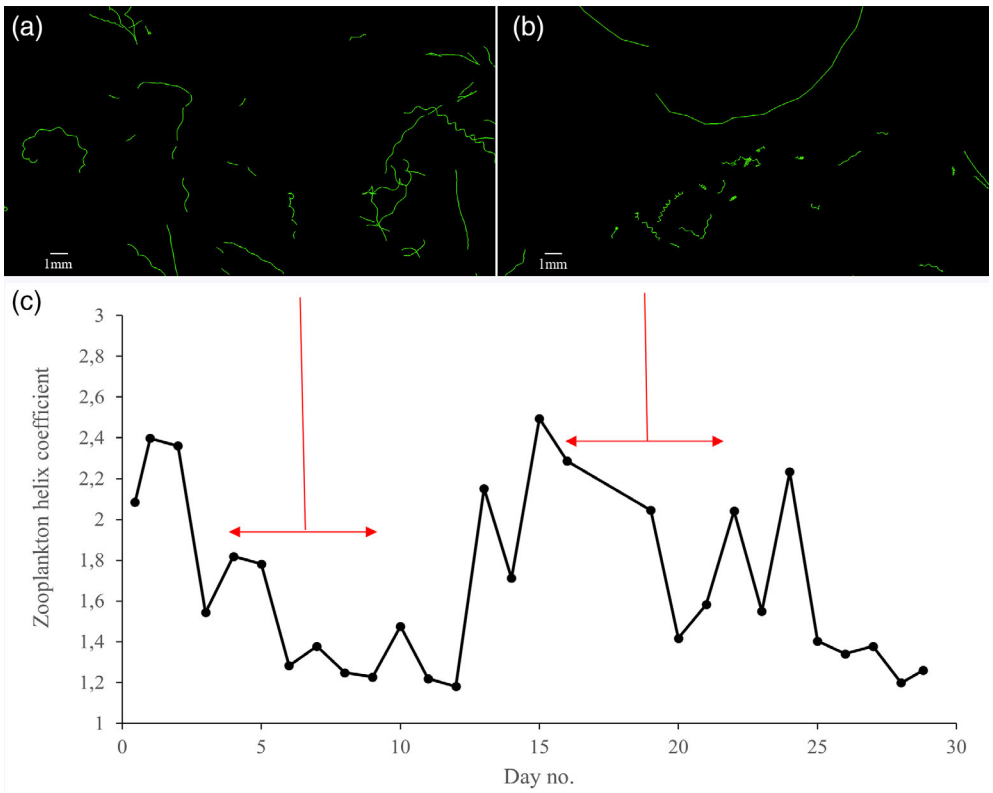

Fig. 8. (**a**) Accumulated swimming tracks during the rotifer-dominated phase, Days 4–9. (**b**) Accumulated swimming tracks during the phase dominated by copepod nauplii and copepodita, Days 16–22. (**c**) Daily community averaged helix coefficient for zooplankton. Red arrows indicate intervals of rotifer (Days 4–9) and copepod nauplii (Days 16–22) dominance.

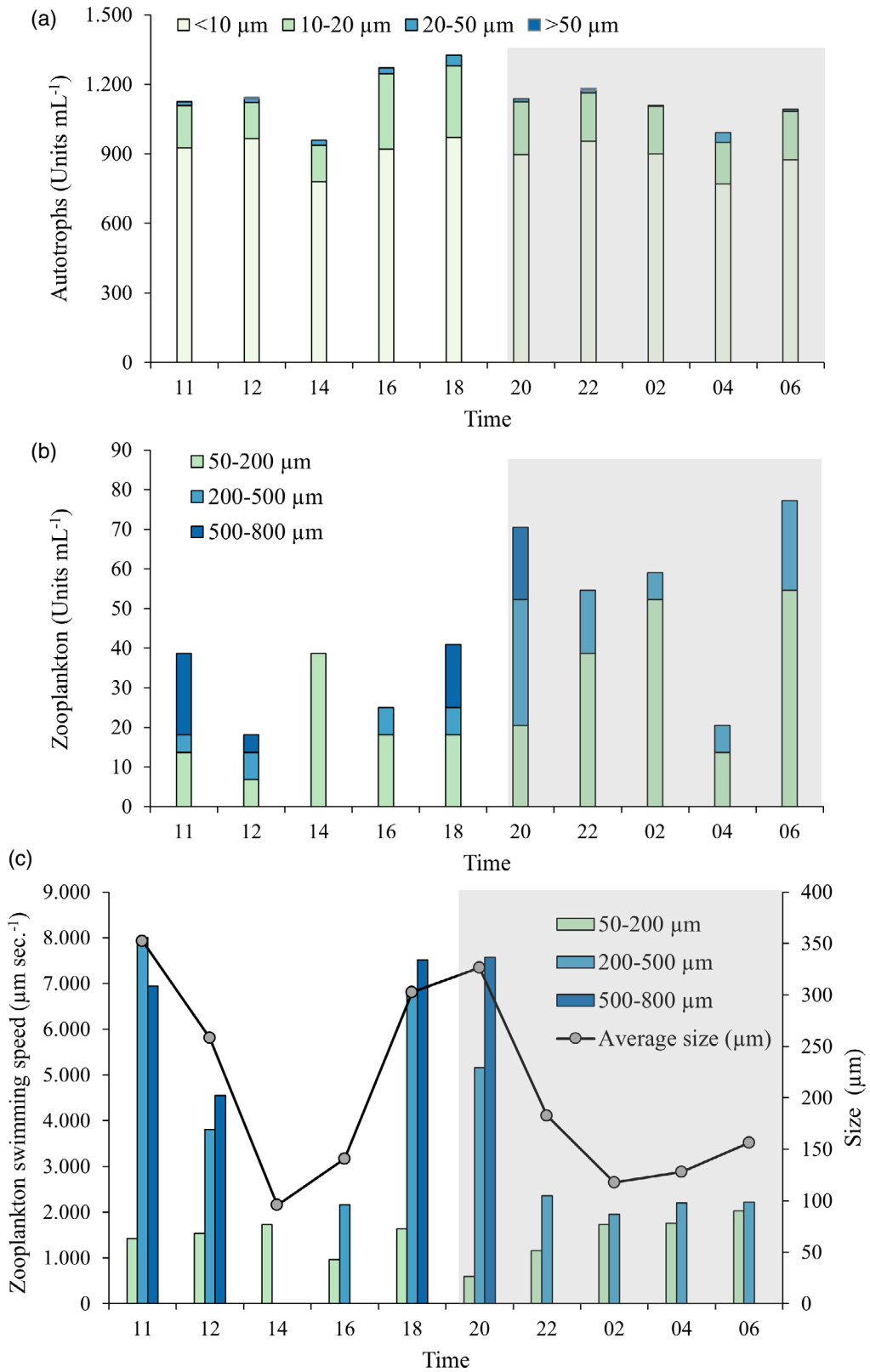

Fig. 9. High resolution phytoplankton dynamics over the course of a day. The dark period is indicated by shading. (**a**) Automatic phytoplankton counts in size classes, (**b**) automatic zooplankton counts in size classes. (**c**) Zooplankton swimming speeds in size classes (bar graph) together with average sizes (line graph).

Zooplankton

Microscopy analysis revealed that the zooplankton community was mostly dominated by the copepod species *Acartia bifilosa* and *Eurytemora affinis*, rotifers *Keratella* spp., and *Synchaeta* spp., while cladoceran *B. coregoni* were present in low numbers. The succession started from smaller organisms: rotifers, followed by copepod species in naupliar stages, and shifting towards larger copepodites at the end of the experiment. Copepod adults only appeared towards the last week, and cladoceran abundance remained low throughout the whole experiment (Fig. 6a).

Automatically estimated organism abundances agree with those measured manually under the microscope for the smaller organisms only, in the size range 50–200 μm (slope = 1.07, $R^2 = 0.82$). The larger organisms, which start to appear at Day 22 onwards (Fig. 6a) were not recorded on the same days by the automatic counter (Fig. 6b). To explain this difference, it is necessary to understand more about the homogeneity of the water column over height and time. Important aspects of the variation over time were revealed during the diel experiment (*see* below).

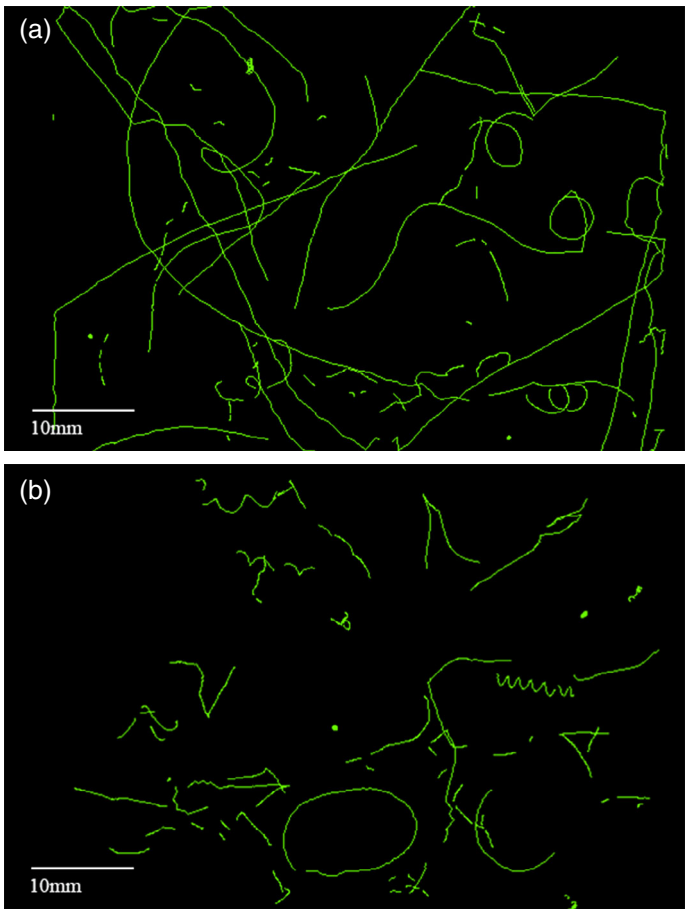

Fig. 10. All accumulated tracks from the two time intervals of lights on (8:00 h to 20:00 h) and lights off (20:00 h to 8:00 h). (**a**) Lights on period. (**b**) Lights off period.

There is generally a strong correlation between body size and swimming speed (Fig. 7) with average swimming speeds approximately 20 times body length, that is, motile organisms typically travel 20 times their length within 1 s. The shift in species from the rotifer-dominated phase in the beginning to the copepod-dominated phase in the end is visible in the appearance of swimming tracks (Fig. 8a,b) as well as the helix coefficient (Fig. 8c). The characteristic tight spiral swimming patterns of copepod nauplii were clearly observed (Fig. 8b) (Titelman and Kiørboe 2003).

Diel experiment

Measurements were performed every second hour over a 20-h period on the last day of the experiment. The phytoplankton counts showed relatively little diurnal variation, as would be expected in a strongly mixed water column (Fig. 9a). The zooplankton community, on the other hand, appeared more varied, where larger organisms (> 500 μm) were found at the sampling point, 80 cm below the surface, during the light hours only, and more specifically only in the first and last hours with daylight (Fig. 9b). Variations in swimming speeds also appeared to be higher in these specific daylight hours (Fig. 9c). Moreover, the higher motility of zooplankton individuals was also visually apparent in the swimming tracks during the light and dark time intervals (Fig. 10).

The mesocosm column was designed to be a mixed water column, however, the exact degree of homogeneity is not easy to quantify, and it appears as though the larger zooplankton were able to overcome the convection currents that result in mixing (Fig. 9c). This is possible since the column took approximately 6 h to reach a mixed state and the scale of water movement is thus of the order 1 m h^{-1}. The larger zooplankton can swim at 8 mm s^{-1} (Fig. 9c) which corresponds to 28 m h^{-1}. This degree of inhomogeneity means that samples must be taken at the same time and location when comparing measurements.

Discussion

There is much yet to understand about the intricate dynamics of microbial ecosystems, which is reflected in the diverse and specialized swimming strategies and sensory apparatus seen in many species. The larger the species, the more sophisticated this apparatus can be, but even the smaller protists can display remarkably complex responses to their environment. It is a goal and a challenge to understand more about this largely invisible world and the niches that exist for survival and fitness optimization (Stocker 2012). Anything that can provide information to this extent is desirable. Experiments undertaken in controlled conditions and based on isolated species have given valuable insight. A few examples of these are Chemotaxis (Fenchel and Blackburn 1999), phototaxis (Tsang et al. 2018), predator evasion (Jakobsen et al. 2006), and predation strategy (Titelman and Kiørboe 2003). However, such studies still represent a subset

of the mechanisms and interactions that exist in natural ecosystems. We suggest a different approach to acquiring data, namely, to measure dynamic properties of ecosystems across a broad range of species and size groups and to extract what information we can from this dataset. Such a dataset, when collected over a variety of environments and environmental conditions will inevitably contain new information on microbial ecosystem structure. For example, we know that some species display different swimming patterns under different conditions (Kiørboe et al. 1996) and we could also expect to record swimming behavior from species known to be able to swim, but whose swimming patterns are not known in detail. Swimming-related measurements are closely related to fitness criteria such as light optimization, predator avoidance, and foraging strategy (Visser 2007). Microorganisms swim in order to utilize niches for growth and to compete for survival, for example, through vertical migration (Schuech and Menden-Deuer 2014). Their movement patterns point therefor towards a particular set of niches available at a point in space and time where a sample is taken (Meunier et al. 2015; Son et al. 2015). All in all, combining behavior-oriented parameters with information regarding environmental state and species composition can provide a more in-depth understanding of a microbial ecosystem.

In theory, the set of coordinates of individual organisms over time contains virtually all the information that is required to document their individual dynamics and, potentially, their mutual interactions. In this study, we have analyzed movement in two dimensions only, but movement is three dimensional. We, therefor, observe a projection of movement onto the plane-of-focus of the camera. This restriction can be overcome to a certain degree by using two cameras placed perpendicular to each other and getting the computer to match tracks from both and thereby construct the true three-dimensional movement (Thar et al. 2000). However, this does limit the volume that is analyzed because the depth of field of one camera must match the field of view of the other. The counting precision of sampling by way of subsamples in the two chambers can be calculated as a Poisson distribution, with intensity parameter (λ) corresponding to the expected number of organisms in the analyzed volume. As an example, with a density of 100 autotrophic cells mL^{-1} (approximately corresponding to the specific size fractions; cf. Fig. 4) analyzed from 20 subsamples in the small chamber (0.024 mL), the number of counted cells will range between 35 and 61 with approximately 95% confidence, corresponding to a density of 100 ± 28 cells mL^{-1}. Similarly, with a density of 20 indv. L^{-1} (approximately corresponding to the total zooplankton abundance; cf. Fig. 6) analyzed from 20 subsamples in the large chamber (0.02 L), the number of counted organisms will range between 3 and 13 with approximately 95% confidence, corresponding to a density of 20 ± 12.5 cells mL^{-1}. The relative precisions of these two examples (28% for autotrophs and 63% for zooplankton) will decrease or increase with higher and lower densities, respectively. Sampling statistics can be improved significantly by concentrating a sample prior to analysis. Although this could be automated, it complicates the setup, and it would likely disturb some aspects of the community and cell interaction. It is an advantage to view as large a volume as possible seen from a statistical point of view, but also for capturing events such as swarming around chemical gradients and mutual interactions between organisms (Harvey et al. 2013). Such events are known to occur, but they are normally difficult to observe in nature. The proposed method of recording sequences over time offers a means of recording such events, and trawling algorithms could search for them in larger databases.

To monitor the full spectrum of plankton from small phytoplankton and protists to larger zooplankton, an instrument must span several orders of magnitude in organism size detection from approximately 2–2000 μm. This is not possible for a single optical chamber configuration (Table 1). It is therefore a practical necessity to provide at least two optical chamber size ranges in either a single instrument or as two separate instruments, each with different optical configurations. This requirement is more easily met with low-cost and compact instruments such as the new generations of holographic flow cytometers (Göröks et al. 2018) or the tracking microscope describe here. Both technologies make use of readily available high-quality cameras and optics, LEDs, and powerful minicomputers. In addition, common to both is the use of advanced software, which provides the core technology. From an optical point-of-view, the main difference between the two technologies is the requirement on resolution. Morphological detail requires much higher resolution than does tracking the center of mass of an organism or a simple size measurement. This allows the tracking microscope to target smaller organisms at the same resolution, which also improves relative sampling accuracy since smaller organisms are typically more abundant than larger organisms.

The tracking microscope technology is scalable in several ways and the current implementation can be upgraded as new technology becomes available. There are already more powerful computers and better cameras than were used in this study and they are continuously getting even better and less costly. As resolution increases, so does the ability to extract more detailed morphological information. More detail, however, requires faster shutter speeds to avoid motion blur which, in turn, requires higher intensity and more focused light on the field of view, preferably together with better control over convection currents within the optical chambers. Dual sensor cameras are available for recording fluorescence in different wavelengths simultaneously (https://www.jai.com/products/product-lines/flex-eye-concept, accessed 27 June 2022). An example of such use is to detect swimming organisms that do not contain Chl *a* by illuminating in blue/violet light and tracking organisms that are swimming without a high-pass filter while simultaneously tracking them as autotrophs through

a high-pass filter to image the presence or absence of Chl *a* fluorescence.

The aim of this study was to demonstrate that the challenge of recording plankton behavior in the field can be met through a mechanical assembly of readily available components, which include industrial video cameras, optics, peristaltic pumps, a microcontroller, LEDs, and a computer. Software provides the intelligence required to identify, measure, and track the movements of organisms. The resulting stream of coordinates in time for each individual represents important information for documenting behavior. It would be ideal to track in all three dimensions but until we can achieve a deep enough field optically for practical purposes, we can extract much information from two-dimensional projections as we have shown. As is the case with all monitoring, the value of data increases with the amount of data available from different environments and under different conditions. In that respect, it makes sense to align monitoring programs around the world in order to accommodate merging data into a common database and provide the possibility of researching behavior-oriented traits in microbial ecosystems directly from field data.

References

Båmstedt, U., and H. Larsson. 2018. An indoor pelagic mesocosm facility to simulate multiple water-column characteristics. Int. Aquat. Res. **10**: 13–29. doi:10.1007/s40071-017-0185-y

Benfield, M., and others. 2007. RAPID: Research on automated plankton identification. Oceanography **20**: 172–187. doi:10.5670/oceanog.2007.63

Brewin, R. J. W., and others. 2019. Factors regulating the relationship between Total and size-fractionated chlorophyll-*a* in coastal waters of the Red Sea. Front. Microbiol. **10**: 1964. doi:10.3389/fmicb.2019.01964

Culverhouse, P. F., C. Gallienne, R. Williams, and J. Tilbury. 2015. An instrument for rapid mesozooplankton monitoring at ocean basin scale. J. Mar.Biol. Aquacult. **1**: 1–11. doi:10.15436/2381-0750.15.001

Dashkova, V., D. Malashenkov, N. Poulton, I. Vorobjev, and N. Barteneva. 2017. Imaging flow cytometry for phytoplankton analysis. Methods **112**: 188–200. doi:10.1016/j.ymeth.2016.05.007

Davis, C. S., S. M. Gallager, M. S. Berman, L. R. Haury, and R. J. Strickler. 1992. The video plankton recorder (VPR): Design and initial results. Arch. Hydrobiol. Beih. Ergebn. Limnol. **36**: 67–81.

Fenchel, T., and N. Blackburn. 1999. Motile chemosensory behaviour of phagotrophic protists: Mechanisms for efficiency in congregating at food patches. Protist **150**: 325–336. doi:10.1016/S1434-4610(99)70033-7

Göröcs, Z., and others. 2018. A deep learning-enabled portable imaging flow cytometer for cost-effective, high-throughput, and label-free analysis of natural water samples. Light: Sci. Appl. **7**: 66. doi:10.1038/s41377-018-0067-0

Harvey, E. L., H. J. Jeong, and S. Menden-Deuer. 2013. Avoidance and attraction: Chemical cues influence predator-prey interactions of planktonic protists. Limnol. Oceanogr. **58**: 1176–1184. doi:10.4319/lo.2013.58.4.1176

HELCOM. 2021*a*. Guidelines for monitoring of phytoplankton species composition, abundance and biomass. HELCOM Monitoring Manual [accessed 2022 June 27]. Available from https://helcom.fi/wp-content/uploads/2020/01/HELCOM-Guidelines-for-monitoring-of-phytoplankton-species-composition-abundance-and-biomass.pdf

HELCOM. 2021*b*. Guidelines for monitoring of mesozooplankton. HELCOM Monitoring Manual [accessed 2022 June 27]. Available from https://helcom.fi/wp-content/uploads/2019/08/Guidelines-for-monitoring-of-mesozooplankton.pdf

Holmstrup, M., P. Haecky, and N. Blackburn. 2020. Preliminary verification studies of the motility and fluorescence assay (MFA) for ballast water quality monitoring. J. Sea Res. **159**: 101889. doi:10.1016/j.seares.2020.101889

Jakobsen, H. H., L. M. Everett, and S. L. Strom. 2006. Hydromechanical signaling between the ciliate *Mesodinium pulex* and motile protist prey. Aquat. Microb. Ecol. **44**: 197–206. doi:10.3354/ame044197

Kiørboe, T., E. Saiz, and M. Viitasalo. 1996. Prey switching behaviour in the planktonic copepod *Acartia tonsa*. Mar. Ecol. Prog. Ser. **143**: 65–75. doi:10.3354/meps143065

Meunier, C. L., K. Schulz, M. Boersma, and A. M. Malzahn. 2015. Impact of swimming behaviour and nutrient limitation on predator–prey interactions in pelagic microbial food webs. J. Exp. Mar. Biol. Ecol. **446**: 29–35. doi:10.1016/j.jembe.2013.04.015

Olenina, I., and others. 2006. Biovolumes and size-classes of phytoplankton in the Baltic Sea. HELCOM Baltic Sea Environment Proceedings. Available from https://epic.awi.de/id/eprint/30141/1/bsep106.pdf

Olson, R. J., and H. M. Sosik. 2007. A submersible imaging-in-flow instrument to analyze nano-and microplankton: Imaging FlowCytobot. Limnol. Oceanogr.: Methods **5**: 195–203. doi:10.4319/lom.2007.5.195

Picheral, M., L. Guidi, L. Stemmann, D. M. Karl, G. Iddaoud, and G. Gorsky. 2010. The Underwater Vision Profiler 5: An advanced instrument for high spatial resolution studies of particle size spectra and zooplankton. Limnol. Oceanogr.: Methods **8**: 462–473. doi:10.4319/lom.2010.8.462

Pitois, S. G., P. Bouch, V. Creach, and J. van der Kooij. 2016. Comparison of zooplankton data collected by a continuous semi-automatic sampler (CALPS) and a traditional vertical ring net. J. Plankton Res. **38**: 931–943. doi:10.1093/plankt/fbw044

Reid, P., J. M. Colebrook, J. B. L. Matthews, J. C. Wright, J. Aikend, and Continuous Plankton Recorder Team. 2003. The continuous plankton recorder: Concepts and history,

from plankton indicator to undulating recorders. Prog. Oceanogr. **58**: 117–173. doi:10.1016/j.pocean.2003.08.002

Schuech, R., and S. Menden-Deuer. 2014. Going ballistic in the plankton: Anisotropic swimming behavior of marine protists. Limnol. Oceanogr.: Fluids Environ. **4**: 1–16. doi:10.1215/21573689-2647998

Schulz, J., and others 2009. Lightframe On-sight Key species Investigation (LOKI). OCEANS 2009-EUROPE. doi:10.1109/OCEANSE.2009.5278252

Son, K., D. R. Brumley, and R. Stocker. 2015. Live from under the lens: Exploring microbial motility with dynamic imaging and microfluidics. Nat. Rev. Microbiol. **13**: 761–775. doi:10.1038/nrmicro3567

Stocker, R. 2012. Marine microbes see a sea of gradients. Science **338**: 628–633. doi:10.1126/science.1208929

Thar, R., N. Blackburn, and M. Kühl. 2000. A new system for three-dimensional tracking of motile microorganisms. Appl .Environ. Microbiol **66**: 2238–2242. doi:10.1128/AEM.66.5.2238-2242.2000

Titelman, J., and T. Kiørboe. 2003. Motility of copepod nauplii and implications for food encounter. Mar. Ecol. Prog. Ser. **247**: 123–135. doi:10.3354/meps247123

Tsang, A. C. H., A. T. Lam, and I. H. Riedel-Kruse. 2018. Polygonal motion and adaptable phototaxis via flagellar beat switching in the microswimmer *Euglena gracilis*. Nat. Phys. **14**: 1216–1222. doi:10.1038/s41567-018-0277-7

Utermöhl, H. 1958. Zur Vervollkommnung der quantitativen Phytoplankton-Methodik. Int. Verein. Theor. Angew. Limnol. **9**: 1–38. doi:10.1080/05384680.1958.11904091

Visser, A. 2007. Motility of zooplankton: Fitness, foraging and predation. J. Plankton Res. **29**: 447–461. doi:10.1093/plankt/fbm029

Willén, T. 1962. Studies on the phytoplankton of some lakes connected with or recently isolated from the Baltic. Oikos **13**: 169–199. doi:10.2307/3565084

Acknowledgments

The study was financed by the EU project Aquacosm (Grant agreement 731065, project CYANOWEB) and the Swedish marine strategic research program EcoChange. Umeå Marine Sciences Centre is gratefully acknowledged for providing mesocosm laboratory facilities.

Conflict of Interest

None declared.

Submitted 22 December 2021
Revised 27 August 2022
Accepted 18 September 2022

Associate editor: Malinda Sutor